TU Delft

Delft University of Technology

Document Version
Final published version

Licence
CC BY-NC-ND

Citation (APA)
Muscari, C., Schito, P., Viré, A., Zasso, A., & van Wingerden, J. W. (2024). The effective velocity model: An improved approach to velocity sampling in actuator line models. *Wind Energy*, *27*(5), 447-462. https://doi.org/10.1002/we.2894

Important note
To cite this publication, please use the final published version (if applicable).
Please check the document version above.

Copyright
In case the licence states “Dutch Copyright Act (Article 25fa)”, this publication was made available Green Open Access via the TU Delft Institutional Repository pursuant to Dutch Copyright Act (Article 25fa, the Taverne amendment). This provision does not affect copyright ownership.
Unless copyright is transferred by contract or statute, it remains with the copyright holder.

Sharing and reuse
Other than for strictly personal use, it is not permitted to download, forward or distribute the text or part of it, without the consent of the author(s) and/or copyright holder(s), unless the work is under an open content license such as Creative Commons.

Takedown policy
Please contact us and provide details if you believe this document breaches copyrights.
We will remove access to the work immediately and investigate your claim.

This work is downloaded from Delft University of Technology.

Check for updates

Received: 8 May 2023 | Revised: 19 October 2023 | Accepted: 20 December 2023

DOI: 10.1002/we.2894

RESEARCH ARTICLE

WILEY

The effective velocity model: An improved approach to velocity sampling in actuator line models

Claudia Muscari[1,2] | Paolo Schito[2] | Axelle Viré[3] | Alberto Zasso[2] | Jan-Willem van Wingerden[1]

[1]DCSC, TU Delft, Delft, The Netherlands

[2]DMecc, Politecnico di Milano, Milano, Italy

[3]FPT, TU Delft, Delft, The Netherlands

Correspondence
Claudia Muscari, DCSC, Delft, The Netherlands.
Email: claudia.muscari94@gmail.com

Funding information
This research received no external funding.

Abstract

Actuator line modeling of wind turbines requires the definition of a free-stream velocity in a computational mesh and a regularization kernel to project the computed body forces onto the domain. Both choices strongly influence the results. In this work, a novel velocity sampling method—the so-called effective velocity model (EVM)—is implemented in the CFD software SOWFA, validated, and compared to pre-existing approaches. Results show superior method robustness with respect to the regularization kernel width (ϵ) choice while preserving acceptable accuracy. In particular, the power predicted by the EVM is nearly independent of the ϵ value.

KEYWORDS
actuator line model, CFD, LES, regularization kernel, velocity sampling, wind turbine modeling

1 | INTRODUCTION

1.1 | Context

The urge to steer away from fossil energy sources is as clear as ever for political and environmental reasons. Currently, the European Union (EU) Institutions and the member states are targeting net zero greenhouse gas emissions by 2050,[1] and wind energy is set to play a big role in this transition.

After decades of research and thanks to the knowledge inherited from the aeronautics field, wind technology is particularly mature, but we still have margins for improvement on many fronts. We can make better use of the favorable sites available for wind plant installation with effective layout and control of the plant itself. To do that, however, we need better models at all fidelity levels.

1.2 | Motivation and challenges

Any technical progress requires the support of data. This data can be obtained via experiments, but for wind energy applications, that is difficult and costly. This is why numerical simulations and, thus, reliable high-fidelity models (usually CFD ones based on the Navier–Stokes equations) are needed.

Given the large Reynolds numbers and the multiple length scales involved, for wind turbines, let alone wind farms, direct numerical simulation (DNS) is unfeasible, and large eddy simulation (LES) on a fully resolved geometry is too computationally demanding to be used extensively.

This is an open access article under the terms of the Creative Commons Attribution-NonCommercial-NoDerivs License, which permits use and distribution in any medium, provided the original work is properly cited, the use is non-commercial and no modifications or adaptations are made.
© 2024 The Authors. *Wind Energy* published by John Wiley & Sons Ltd.

An alternative to fully blade/turbine-resolved simulations is to parameterize the effect of the turbine on the flow. This can be achieved by means of body forces properly computed and projected into the flow field. The most popular approaches are the actuator disk model (ADM) and the actuator line model (ALM). The latter was introduced in Sorensen and Shen[2] and has since been validated,[3] improved,[4] discussed and compared to other methods[5] on many occasions.

The ALM can be very reliable, provided the user is particularly cautious in setting the model parameters. In fact, result quality can vary dramatically with grid resolution, projection function width, and velocity sampling method.[6] In particular, the value of the projection function width, ϵ, needs to be tuned, and the definition of the so-called free-stream velocity is ambiguous.

Another notion worth mentioning is the one of tip loss correction, which is needed because, in principle, the ALM is based on one-dimensional momentum theory in which forces are distributed continuously in the azimuth direction, corresponding to an infinite number of blades with no tip loss. The most commonly used correction is named after Prandtl,[7] but more advanced options are available.[8] Tip losses are also connected to the regularization kernel in the sense that choices different from the standard 3D Gaussian function could result in a more realistic flow configuration at the tip.

These issues combined commonly result in difficulties in simultaneously predicting turbine power and thrust with this approach, which also impacts the prediction of the wake deficit downstream of the rotor.

1.3 | Projection function width

A variety of rules for the choice of ϵ have been adopted in the literature. For example, it can be set to twice the cell dimension in the rotor area,[6] which is a good rule of thumb only when considering big rotors. Others have tried to relate the value of ϵ to geometric quantities rather than having it as a function of spatial resolution. This can be done, for example, by setting ϵ equal to 0.035 times the rotor diameter,[4] which requires very high resolutions or have its value vary along the blade and be equal to a quarter of the airfoil chord at that station.[9] Assuming as ground truth the chord-dependent ϵ definition, Martinez-Tossas and Meneveau[10] obtained, analytically, a subfilter scale velocity model able to attain optimal accuracy with suboptimal kernel sizes.

1.4 | Free-stream velocity

The main variable in ALM implementations is the free-stream velocity, used to evaluate the angle of attack and to dimensionalize the aerodynamic forces. We know that the sampled free-stream velocity should contain the deceleration caused by the rotor induction but not the blade-local flow effects.[4]

Blade Element Momentum (BEM) methods normally use the undisturbed flow velocity. This approach is not very accurate, as the effects of induction are neglected, and the distance at which the sampling is done is a tunable parameter. With the whole flow field accessible in hybrid analytical-CFD solvers, the most obvious idea is to sample in the center of the cell containing the actuator line point (local sampling).

This idea is based on the assumption that the actuator line point is located at the center of the bound vortex cross-section, where the effect of the bound vortex itself is null.[11] The validity of this assumption is questionable for two reasons. First of all, a fundamental objection comes from the fact that Biot–Savart and Kutta–Joukowski's laws are formulated in potential flow theory, which can hardly be representative of a wind turbine's operating conditions and does not hold when using kernel functions different than the classic isotropic Gaussian one. Moreover, the lift generated by the bound vortex causes a local velocity angle increase (up-wash) in front of the considered point and a decrease (down-wash) behind it, meaning that there will be a strong gradient in velocity angle and that a small error in the sampling results in significant errors in angle evaluation.

Shives and Crawford[12] showed that this error, in CFD simulations, is always non-zero and that its magnitude depends strongly on grid resolution. They introduced the idea that the velocities induced across an actuator line resemble the ones predictable with a viscous vortex core model. Dag[13] further elaborated on that idea, demonstrating a very good agreement between a Lamb–Oseen[14] vortex core model and AL swirl velocities. Significant progress was made by Meyer Forsting et al,[15] who gave theoretical and practical proof of the fact that smearing the forces in AL models produces a viscous core in the bound and shed vorticity of the line and suggested a vortex-based correction. In a follow-up paper,[16] Meyer Forsting and Troldborg found that the error in the evaluated lift depends on the chord, on ϵ, and on the $\epsilon/\Delta x$ ratio. The subfilter-scale velocity correction presented in Martínez-Tossas and Meneveau[10] and shortly introduced in Section 1.3 can also be seen as a variant of a vortex-based correction. Kleine et al[17] observed that these methodologies introduce an error dependent on the difference of circulation between time steps and on the weighting/relaxation factors used.

Alternatives to local sampling with and without corrections are numerous and typically involve averaging over multiple cells or time steps. Recent examples include the Lagrangian sampling[18] and the integral method.[4] The latter is considered state-of-the-Art and will be described in Section 2.2.

10991824, 2024, 5, Downloaded from https://onlinelibrary.wiley.com/doi/10.1002/we.2894 by Tu Delft, Wiley Online Library on [02/05/2024]. See the Terms and Conditions (https://onlinelibrary.wiley.com/terms-and-conditions) on Wiley Online Library for rules of use; OA articles are governed by the applicable Creative Commons License

1.5 | Research objectives and work outline

The gap we would like to fill with this study is to provide an elegant solution to both the mentioned issues at the same time:

1. evaluate the velocity in a way that is at the same time consistent with the physics and compatible with the numerics;
2. overall, make the turbine model less dependent on the ϵ value.

This is achieved by implementing the effective velocity model (EVM) in SOWFA, which is currently the state-of-the-art framework for AL simulations.

The EVM was first introduced in Schito and Zasso,[19] implemented on the Politecnico di Milano in-house AL code, and then used with success in following studies on both vertical axis[20] and horizontal axis[21] wind turbines. The reason for implementing the EVM in SOWFA was that, although the two codes have comparable accuracy and computational speed, SOWFA is more complete (atmospheric boundary layer solver, coupling with FAST) and more widely spread (which also means more widely tested).

In this paper, we validate our implementation in SOWFA against BEM results and other actuator line models. We then assess the performance of our sampling method against local sampling and integral sampling[4] in predicting rotor performances (power and thrust), reducing spurious oscillations in the local quantities (axial velocity and angle of attack), and evaluating the wake velocity deficit.

The paper is organized as follows. Section 2 presents SOWFA and its ALM solver, then the EVM and its implementation. Section 3 describes the setup of the simulations of the DTU 10 MW turbine used for validation and comparison. In Section 4, results are shown and discussed. Finally, conclusions are drawn in Section 5.

2 | METHODS AND TOOLS

This section first shortly introduces the actuator line model and gives a brief overview of SOWFA and its velocity sampling methods. Then, the motivation behind the EVM, the process behind its synthesis, and its implementation are described.

2.1 | Actuator line model

The actuator line model (ALM) was developed in order to overcome the limitations of the axisymmetric actuator disk (AD), a concept that was already present in the basic aerodynamic description of wind turbines. The biggest limitation of AD is that, since the force distribution is uniform on the disk, the influence of the blade is taken as an integrated quantity in the azimuthal direction. With the ALM, the forces, instead of being distributed uniformly on the disk, are applied to the flow field along rotating lines that correspond to the individual rotor blades. They can be modeled in a way that allows them to respond dynamically to changing conditions and can account for aeroelasticity when coupled to a structural code. This allows us to describe the wake's dynamics better and capture the tip vortexes and their influence on the induced velocities. However, smaller-scale phenomena, such as those involving the blade boundary layer, cannot be captured. That is the main disadvantage with respect to a fully resolved geometry, but also what makes it so computationally convenient since the description of the blades' boundary layer would require a much more complex mesh. Moreover, LES, which have been reported to present issues in the treatment of the near-wall region,[22] can now be used more reliably. Two crucial aspects of the AL that differentiate the many models available are

- the sampling of the freestream velocity and
- the projection of the body force.

The sampled free-stream velocity $\overrightarrow{V_{rel}^{2D}}$ (we specified "2D" because, in the model, a two-dimensional airfoil is considered) is necessary to compute the angle of attack α). The variables in the following equations are shown in Figure 1.

$$\overrightarrow{V_{rel}^{2D}} = \overrightarrow{V_\infty} - \omega r \vec{t} = V_\infty \vec{n} + (V_\infty - \omega r)\vec{t} \tag{1}$$

$$\vec{L} = \frac{1}{2}\rho \left(\overrightarrow{V_{rel}^{2D}}\right)^2 C_L(\alpha) c \vec{l} \tag{2}$$

$$\vec{D} = \frac{1}{2}\rho \left(\overrightarrow{V_{rel}^{2D}}\right)^2 C_D(\alpha) c \vec{d} \tag{3}$$

10991824, 2024, 5, Downloaded from https://onlinelibrary.wiley.com/doi/10.1002/we.2894 by Tu Delft, Wiley Online Library on [02/05/2024]. See the Terms and Conditions (https://onlinelibrary.wiley.com/terms-and-conditions) on Wiley Online Library for rules of use; OA articles are governed by the applicable Creative Commons License

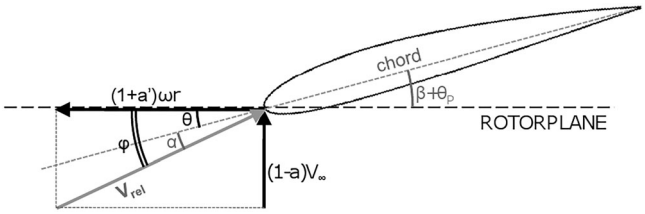

FIGURE 1 Velocities at the rotor plane.

$$\phi = \angle \overrightarrow{V_{\text{rel}}^{2D}} \tag{4}$$

$$\alpha = \phi - \beta, \tag{5}$$

where $\overrightarrow{V_\infty}$ is the undisturbed wind speed, ω is the rotor speed in rpm, r is the radial distance from the hub, $\vec{t}$ and $\vec{n}$ are the tangential and normal vector, respectively, $\vec{L}, \vec{D}, C_L$ and C_D are the lift and drag forces and the lift and drag coefficients, respectively, and ρ is the density of air. The angle ϕ is the flow angle, and β is the twist of the blade. A common choice for evaluating $\overrightarrow{V_{rel}^{2D}}$ is sampling it directly in the cell containing the actuator line point.

The projection function is needed to smear the computed force over multiple cells. The most physical solution would be to apply them in the single cell containing the airfoil pressure center. However, this could be mathematically problematic since the sharp gradient generated could lead to strong spurious oscillations in the vicinity of the actuator line. The most common choice is to use a three-dimensional Gaussian smearing function that is isotropic in width and fixed along the blade span.[3] This makes the resultant body force field around an actuator line appear like a cylindrical cloud surrounding the line. The function can be written as follows:

$$\eta^{RK}(r) = \frac{1}{\epsilon^3 \pi^{\frac{3}{2}}} \exp - \left(\frac{d^2}{\epsilon^2}\right) \tag{6}$$

where d represents the distance of the considered cell from the application point and ϵ is the width of the Gaussian distribution. In every domain cell, the total inserted force will be equal to the following:

$$f(x) = \sum_i f^i \eta^{RK} |x - x^i| \tag{7}$$

2.2 | SOWFA

SOWFA[23] is a set of libraries, solvers, boundary conditions, and tools specific to wind turbine simulations and constitutes an extension of OpenFOAM. It was originally developed at the National Renewable Energy Laboratory (NREL) and can be coupled to the structural solver of NREL's wind engineering tool OpenFAST. SOFWA solves the Navier-Stokes equations numerically using, for example, a Pressure Implicit with Split Operator (PISO) algorithm. The latter is modified with the addition of body forces that parametrize the effect of the wind turbine on the flow using a state-of-the-art ALM, and an atmospheric boundary layer (ABL) solver that allows running precursor simulations to provide a turbulent inflow to wind farm simulations. The linear systems that arise when discretizing the implicit equations are solved using preconditioned iterative solvers.

SOWFA's ALM provides three different sampling methods, represented in Figure 2, for the free-stream velocity:

- cellCenter: considering the current point of the actuator line, it uses the value at the nearest neighbor cell center;
- linear: uses linear interpolation from the cell within which the point lies and neighboring cells;
- integral: determines the free-stream velocity using an integral of the velocity field weighted by the force projection function.[4]

Concerning the projection function itself, the only option currently implemented is the already described isotropic three-dimensional Gaussian.

10991824, 2024, 5, Downloaded from https://onlinelibrary.wiley.com/doi/10.1002/we.2894 by Tu Delft, Wiley Online Library on [02/05/2024]. See the Terms and Conditions (https://onlinelibrary.wiley.com/terms-and-conditions) on Wiley Online Library for rules of use; OA articles are governed by the applicable Creative Commons License

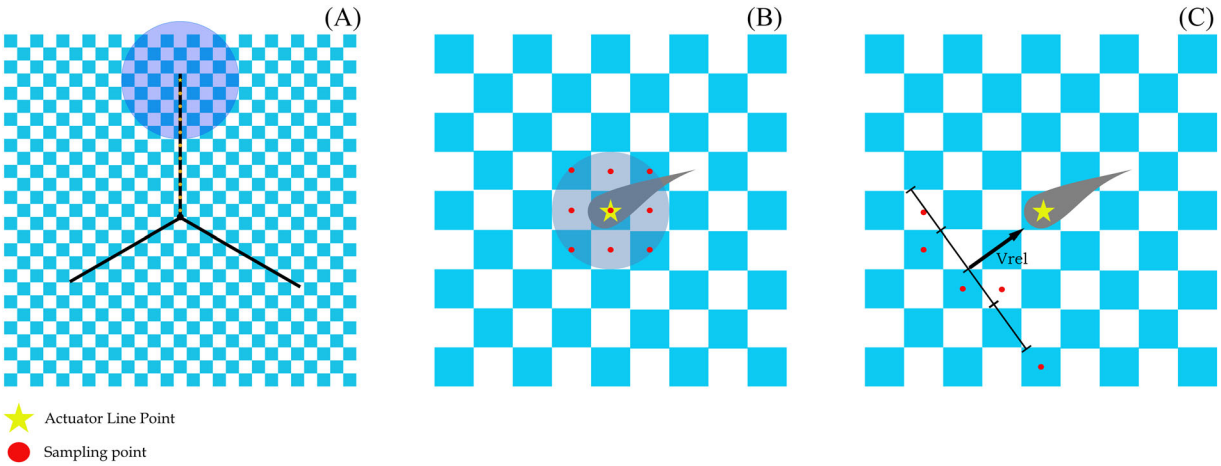

FIGURE 2 The first sub-figure (A) represents the rotor plane and the blade discretization. The purple circle in sub-figure a is actually a sphere and corresponds to the gray one in sub-figure b. It is centered on a given actuator line point and has a radius equal to ϵ. Sub-figures (B) and (C) zoom in on a single actuator line point and show how the sampling happens. In particular, we have a representation of the integral sampling (B) and of the EVM sampling (C). In sub-figure (B), the sampling points are the centers of the cells intersected by the gray sphere. In sub-figure (C), the sampling line is perpendicular to the relative velocity, one cell and a half upstream from the chosen actuator line point and five cells long.

2.3 | The effective velocity model

The main idea behind the EVM is that it is better to evaluate the angle of attack α and the effective velocity on the rotor plane by averaging the velocity sampled on a segment, and thus on multiple points, rather than sampling a single point like in the local approach. The segment is positioned slightly upstream of the rotor and perpendicular to the mean relative velocity direction.

Like the integral approach, the EVM is based on spatial averaging. This can be particularly suitable for turbulent cases where the entire unsteady incoming flow information cannot be characterized with a single sample. As explained in Section 1.4, the weakness of the more straightforward local approach comes from the assumption of null vortex-induced velocity in the sampling point.

The synthesis of the EVM required a definition of the sampling segment in terms of position (with respect to the considered actuator line point), length, and direction (with respect to both the blade and the incoming flow) and an evaluation of how sampling slightly upstream might change the angle of attack. The model is semi-empirical since these quantities had to be tuned experimentally.

The calibration was done through 2D simulations of a NACA0012 airfoil at different angles of attack. The angle of attack for a blade section typically varies between 0° and 10°, so for the calibration, $\alpha_\infty = 3^\circ, 6^\circ, 9^\circ$ was considered. It was documented, together with the implementation of the EVM in an in-house AL code from Politecnico di Milano, by Bernini and Caccialanza in their Master thesis[24] in Schito and Zasso.[19] It resulted in the following:

- Distance: the optimal value for the distance between the sampling line and the actuator line was found to be equal to 1.5 h_{cell} where h_{cell} is the characteristic cell dimension. This value was obtained through a comparison between AL and a fully resolved simulation on a test airfoil at fixed wind conditions as the one that minimized the error in the evaluation of the effective velocity;
- Direction: the direction of the sampling line is orthogonal to the mean relative velocity direction. This way, spurious contributions coming from the translational motion can be avoided;
- Length: the obtained optimal value for the sampling line length is 5 h_{cell}. The optimization procedure follows the same approach we have seen for the distance, but this time the focus is on the angular deviation of the flow from the undisturbed one.
- Correction for the angle of attack:

$$\begin{cases} v_\infty = v_{EVM} \\ \Delta\alpha = \alpha_{EVM} - \alpha_\infty = \dfrac{c}{h_{cell}}(1.2553 - 0.0552 C_D) C_L \end{cases} \tag{8}$$

This correction quantifies the distortion induced on the flow by the wind-blade interaction at the sampling distance. The module of the velocity does not vary. The angle of attack increases with the intensity of the bound vorticity (so proportionally to the lift coefficient). One thing to be

10991824, 2024, 5, Downloaded from https://onlinelibrary.wiley.com/doi/10.1002/we.2894 by Tu Delft, Wiley Online Library on [02/05/2024]. See the Terms and Conditions (https://onlinelibrary.wiley.com/terms-and-conditions) on Wiley Online Library for rules of use; OA articles are governed by the applicable Creative Commons License

remembered is that the obtained correction is valid only for the chosen configuration of the sampling line. In particular, it is inextricably related to the length of the sampling line.

Bernini and Caccialanza,[24] after the calibration and before testing the EVM on a 3D case, demonstrated the effectiveness of the model, respectively:

- on a NACA63.4, an asymmetric airfoil (the NACA0012 was symmetric) and
- with oscillating inflow conditions,

thus extending its validity. Tests were also done with lift and drag combinations in a wide range without considering specific airfoils.

The 3D case that they presented was based on experiments performed in the Politecnico di Milano wind tunnel on the scaled mode of a Vestas V90 3MW wind turbine,[25] which had a rotor diameter of 2 m. The EVM implementation does not change with respect to the 2D case, and at each time step, the incoming velocity for an actuator line point at a given radial position is obtained by averaging the values over the sampling line and correcting the direction as prescribed.

Two meshes with different levels of refinement (0.1 and 0.05 m) were considered at first, and the coarsest was adopted in the following since differences were negligible. The solver was then tested under different tip speed ratios (TSR) and a fixed pitch angle. This resulted in angles of attacks near the stall region and higher discrepancies with the experimental results in correspondence with the lowest TSR.

3 | NUMERICAL SETUP

This section presents the setup used to test the newly implemented method and assess it. We describe the reference turbine and the available data; we then detail every step of the CFD setup and the changes for the various tested configurations.

3.1 | The NREL 5-MW reference turbine and the operating conditions

The "NREL offshore 5-MW baseline wind turbine"[26] (NREL 5-MW) is a reference turbine that was conceptualized including design information from manufacturers and publicly available data from other concepts projects. Researchers in the past decades have widely used it for testing and validating methods. Performance predictions in the original report were obtained with FAST,[27] a modular aero-servo-elastic code. This makes it easy to simulate the turbine in SOWFA since many FAST input files can be easily adapted if not used directly. Table 1 summarizes the main properties of the turbine.

3.2 | Domain and space discretization

In Martinez-Tozzas et al,[28] a standard test case for the NREL 5-MW is defined and simulated with four different AL codes. The considered domain is a parallelepiped with dimensions $24D \times 6D \times 6D$ (with D indicating the turbine diameter), and the turbine hub is positioned $3D$ away from the top, bottom, and inflow plane.

Thanks to the fact that the actuator line does not require the solution of the blade boundary layer, the mesh is almost as simple as it can be: It is obtained with a block mesh and a number of local refinements applied on a cylinder whose base has the same diameter of the turbine and

TABLE 1 NREL 5-MW main geometrical and control parameters.

Rating	5 MW
Rotor orientation, configuration	Upwind, 3 blades
Control	Variable speed, collective pitch
Rotor, hub diameter	126 m, 3 m
Hub height	90 m
Cut-in, rated, cut-out wind speed	3 m/s, 11.4 m/s 25 m/s
Cut-in, rated rotor speed	6.9 rpm, 12.1 rpm
Rated tip speed	80 m/s
Overhang, shaft tilt, precone	5 m, 5°, 2.5°

10991824, 2024, 5, Downloaded from https://onlinelibrary.wiley.com/doi/10.1002/we.2894 by Tu Delft, Wiley Online Library on [02/05/2024]. See the Terms and Conditions (https://onlinelibrary.wiley.com/terms-and-conditions) on Wiley Online Library for rules of use; OA articles are governed by the applicable Creative Commons License

whose length starts from a bit upstream of the turbine and ends at the end of the domain. Each refinement halves the characteristic length of the refined cell.

Developers[23] and users have suggested that there should be at least 20 cells along a rotor radius which become at least 50 if we want to resolve tip/root vortices. The mesh considered for this study has cells with a characteristic dimension of 33.6 m on the outer part of the domain. To this base mesh, we applied four refinements resulting in the characteristics listed in Table 2. Table 3 adds details on the refinement zones, and a simple visualization of the domain is given in Figure 3.

3.3 | Numerical schemes and boundary conditions

SOWFA describes the flow with an unstructured, collocated variable, finite-volume formulation. The accuracy in time and space is second order. The filtered momentum equation is solved along with an elliptic equation for the pressure that enforces continuity. A Smagorinsky subgrid-scale model with a fixed C_s coefficient is used. We impose a uniform inflow with an 8 m/s wind speed and a zero normal pressure gradient at the inlet. At the outlet, we have zero normal gradient of velocity and fixed pressure. The lower surface-boundary conditions are based on Monin and Obukhov[29] similarity theory, which is standard practice in the atmospheric LES community. The upper boundary is a stress-free, rigid lid, and the lateral boundary conditions are set to zero gradient with no penetration. These boundary conditions are summarized in Table 4.

3.4 | Time discretization

The time step must be set correctly to avoid numerical instabilities in the simulation. Here, a Courant–Friedrichs–Lewy (CFL) number based on the rotation speed at the tip of the blade is used to choose an appropriate time step. It is defined as

TABLE 2 Details on the mesh used for the NREL-5MW test case.

Global refinements	**0**
Local refinements	4
Number of cells	9,907,187
Minimum cell dimension $[m]$	2
Cells along rotor	64

TABLE 3 Details on the refinement zones.

Refinement	**1**	**2**	**3**	**4**
$\frac{D_{cylinder}}{D_{rotor}}$	1.5	2	2.5	3
Upstream length	2 D	2.5 D	2.5 D	3 D

Note: The zones are cylindrical, centered at the rotor hub, and extend to the end of the domain. The values on the first line are the ratios between cylinders and rotor diameter, and the ones on the second indicate how far upstream of the rotor plane the zone starts. This distance is expressed in diameters, with $D = 126$ m.

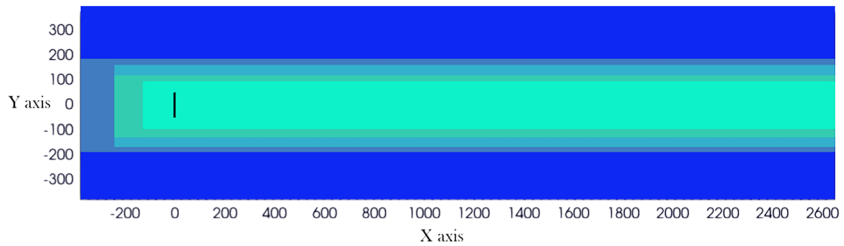

FIGURE 3 Two-dimensional visualization of the domain with the line in black in the middle representing the turbine and the rectangles representing the refinement areas whose dimensions are indicated in Table 2.

10991824, 2024, 5, Downloaded from https://onlinelibrary.wiley.com/doi/10.1002/we.2894 by Tu Delft, Wiley Online Library on [02/05/2024]. See the Terms and Conditions (https://onlinelibrary.wiley.com/terms-and-conditions) on Wiley Online Library for rules of use; OA articles are governed by the applicable Creative Commons License

TABLE 4 NREL 5MW test case boundary conditions.

Patch	U	P	k	nuSgs
Lower	slip	zeroGradient	zeroGradient	zeroGradient
Upper	slip	zeroGradient	zeroGradient	zeroGradient
West	fixedValue	fixedValue	fixedValue	fixedValue
East	inletOutlet	zeroGradient	zeroGradient	zeroGradient
South	slip	zeroGradient	zeroGradient	zeroGradient
North	slip	zeroGradient	zeroGradient	zeroGradient

$$CFL_{tip} = \frac{\omega R \Delta t}{\Delta_g} \tag{9}$$

where ω is the wind turbine rotational speed, R is the blade radius and $\Delta_g = \sqrt[3]{\Delta_x \Delta_y \Delta_z}$ is the equivalent cell dimension.

This choice is motivated by the fact that scaled wind turbines rotate very fast. Maintaining this CFL at a value smaller than one should prevent the blade tip from crossing more than one cell per time step and guarantee an equal number of force calculations per rotor revolution.[30] In fact, if the time step is too large, the forces can be computed asymmetrically or only in specific positions, introducing oscillations of the loads or vibrations of the structure. For all the simulations in this study, we consider a time step of $\Delta t = 0.015$ which always guarantees the respect of the condition.

3.5 | ALM parameters

Actuator line simulations require some additional knowledge for proper implementation with respect to normal CFD ones. As said in Section 3.4, the time discretization must ensure that the blade tip does not cross more than one grid cell per time step. The choice of the correct value for the projection function width ϵ is of the utmost importance in an ALM simulation. If the chosen value is too large, the actuator line model will appear to recover an aerodynamic power above the Betz limit, and if it is too low, the predicted power will be well below measurements or BEM calculations.

Turbine quantities such as lift and drag forces depend heavily on the value of ϵ. In the literature, there is no consensus on how to choose it correctly. Churchfield et al[4] claim that a value of 0.035 times the rotor diameter works well for big enough turbines, Shives and Crawford[12] found it to be optimal when the ratio ϵ/c, where c is the local chord, is equal to 0.25, while in many other works, it has to be tuned to the mesh dimension in the rotor area. In this work, when comparing the sampling methods, the choice was to set ϵ as twice the mesh dimension, as suggested in Sorensen and Shen.[2] The choice adopted in the validation will be made explicit and explained in Section 4.1. This is somewhat far from the optimum defined in Shives and Crawford,[12] but reaching it would require the use of very fine meshes. Other relevant information on the considered simulations is that the chord and twist as a function of the blade radius are linearly interpolated from tabular data. The number of actuator points is 64.

4 | RESULTS

With the setup described in Section 3, several simulations were run with different objectives. The operating conditions are the same as those considered in Martinez-Tozzas et al.[28] In the validation part, this is also the case for the AL parameters. The latter are then modified for the comparison of the different sampling methods. In particular, we compare EVM results to the ones obtained with three other popular sampling methods with a $\frac{\epsilon}{\Delta x}$ equal to two. Finally, we keep the base mesh and focus on the sensitivity to the force projection by varying the ϵ over Δx ratio.

4.1 | Method validation

In Martinez-Tozzas et al.,[28] SOWFA's ALM was validated on the setup described in Section 3 against three different CFD codes: EllipSys3D,[30] LESGO[31] and SP-Wind.[32] The BEM data from the NREL 5-MW report[26] were used as a reference. All cases were run with a fixed value of $\epsilon = 10$, which is very big. This was done to obtain very smooth results. Close agreement of the results among the codes was shown for quantities along the blades and in the near-wake.

10991824, 2024, 5, Downloaded from https://onlinelibrary.wiley.com/doi/10.1002/we.2894 by Tu Delft, Wiley Online Library on [02/05/2024]. See the Terms and Conditions (https://onlinelibrary.wiley.com/terms-and-conditions) on Wiley Online Library for rules of use; OA articles are governed by the applicable Creative Commons License

Neither the CFD simulations nor the BEM code employed tip corrections. The EVM was also previously validated when implemented in the Polimi AL code.[19] Thus, our validation of the EVM implementation in SOWFA was done by means of a cross-comparison with the results of Martinez-Tozzas et al.[28] Figure 4 shows time-averaged quantities along the blade. The quantities compared are the axial velocity, normalized with respect to the inflow velocity U_∞, the angle of attack, and lift and drag forces normalized by length ($F_L^* = F_L/wD\rho U_\infty^2$, where w is the width of the current blade section, ρ is the air density, D is the rotor diameter).

We can observe that, for all the codes considered, the trends in terms of angle of attack and forces are correctly reproduced by our implementation. However, the predicted values of axial velocity differ from the other approaches (Figure 4, top left). This is explained by the fact that, while other codes use some version of the local approach, for the EVM, the velocity shown in Figure 4 is sampled upstream. Thus it is completely normal for it to be significantly higher. This difference is especially relevant in the middle part of the blade.

It is important to understand that this is not the velocity used to compute the forces: the angle of attack must be corrected to take the fact that we are sampling upstream into account: the presence of a profile induces only a deflection on the incoming flow so, while the absolute value of $\overrightarrow{V_{rel}^{2D}}$ will be the same, its axial component will not. We can observe that the angle matches very well the BEM reference, even in the area where the other approaches were not as accurate. Bigger quantitative differences can be spotted in the force prediction, especially the lift. Small differences in the angle of attack result in a significant over-prediction of forces for the traditional methods in the second half of the blade span and in a consistent under-prediction for the EVM along the whole span. Apart from the different sampling, one justification for the significant quantitative differences is that the EVM gives results that are less dependent on the ϵ value (as will be proved in Section 4.3).

4.2 | Comparison between different sampling methods

It is interesting to assess the EVM against the other sampling methods available in SOWFA. To do that, we consider the same setup, but we set the ϵ value to a more reasonable $2\Delta x$. Figure 5 shows the time evolution of the angle of attack evaluated with the four methods on three different points: one located at the blade's root, one in the mid section, and one on the tip.

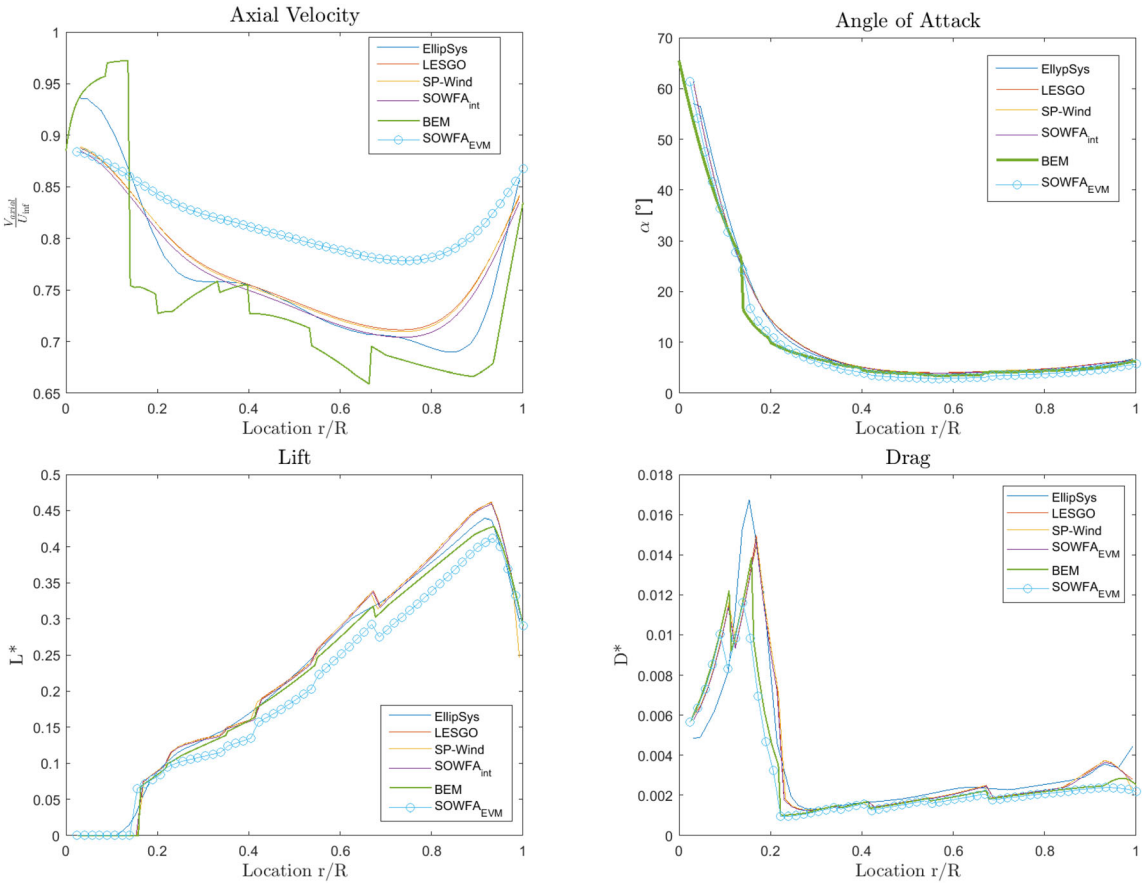

FIGURE 4 Spanwise evolution of the axial velocity (top left, normalized with the inflow velocity), angle of attack (top right), a dimensional lift (bottom left), and drag force (bottom right), evaluated with four different LES codes. The EVM axial velocity is the one sampled upstream and not yet projected with the new angle of attack. All quantities are made non-dimensional. The BEM results are included as a reference.

10991824, 2024, 5, Downloaded from https://onlinelibrary.wiley.com/doi/10.1002/we.2894 by Tu Delft, Wiley Online Library on [02/05/2024]. See the Terms and Conditions (https://onlinelibrary.wiley.com/terms-and-conditions) on Wiley Online Library for rules of use; OA articles are governed by the applicable Creative Commons License

The time-dependent signal is periodic because of the asymmetry of the rotor plane: the nacelle is tilted, and the blades are pre-coned.

Looking at Figure 5, and in general, in time-varying plots, we recognize spurious oscillations. We can observe that, as we move along the blade, they increase in frequency and decrease in amplitude (the blade passes through more cells). These oscillations are always present in AL simulations; they depend strongly on the spatial discretization and chosen sampling method. In that sense, all sampling methods perform better than the cell-centered one: the linear because of interpolation, the EVM, and the integral because of spatial average. For the methods with no spatial average, in Jha et al,[33] the issue was observed and solved by just intervening on the numerics: they started by using different blends of second-order linear and first-order upwind interpolation upstream of the actuator and elsewhere, which worked for a uniform grid (stretched grids require ulterior attention) and did not produce excessive artificial diffusion. Xie[18] also recently tackled the issue by integrating a Lagrangian averaging in time to the sampling.

These oscillations are, thus, only related to the line crossing different cells (the frequency increases toward the tip, where the blades travel faster). We chose not to try to eliminate them since they have no effect on the global quantities that we are interested in.

The subsequent step was to look at the spanwise evolution of the local quantities. The values at each blade station were evaluated by averaging over the last third of the simulation time. Figure 6 shows the evolution of the angle of attack and the axial velocity. The axial velocity is significantly higher. Again (as in Section 4.1), it is the one sampled upstream, not yet corrected and it is not the one used to compute the forces.

Differences among the methods in evaluating the angle of attack can be appreciated when considering fewer actuator line points (it must be noted, though, that these differences become negligible for integral quantities). This is shown in Figure 7.

Figure 8 shows the adimensional lift and drag forces along the span. As in Section 4.1, the lift predicted by the EVM is significantly lower. The drag is very close, but, with the EVM, the peak at around 15% span is not as pronounced. These differences will ultimately translate to differences in the global quantities and in the wake.

While looking at local quantities allows us to understand where the methods differ, ultimately, we are interested in global quantities such as power and thrust. The actuator line quite famously fails at accurately predicting both of them at the same time. The closest it gets to one, the farthest from the other.[34]

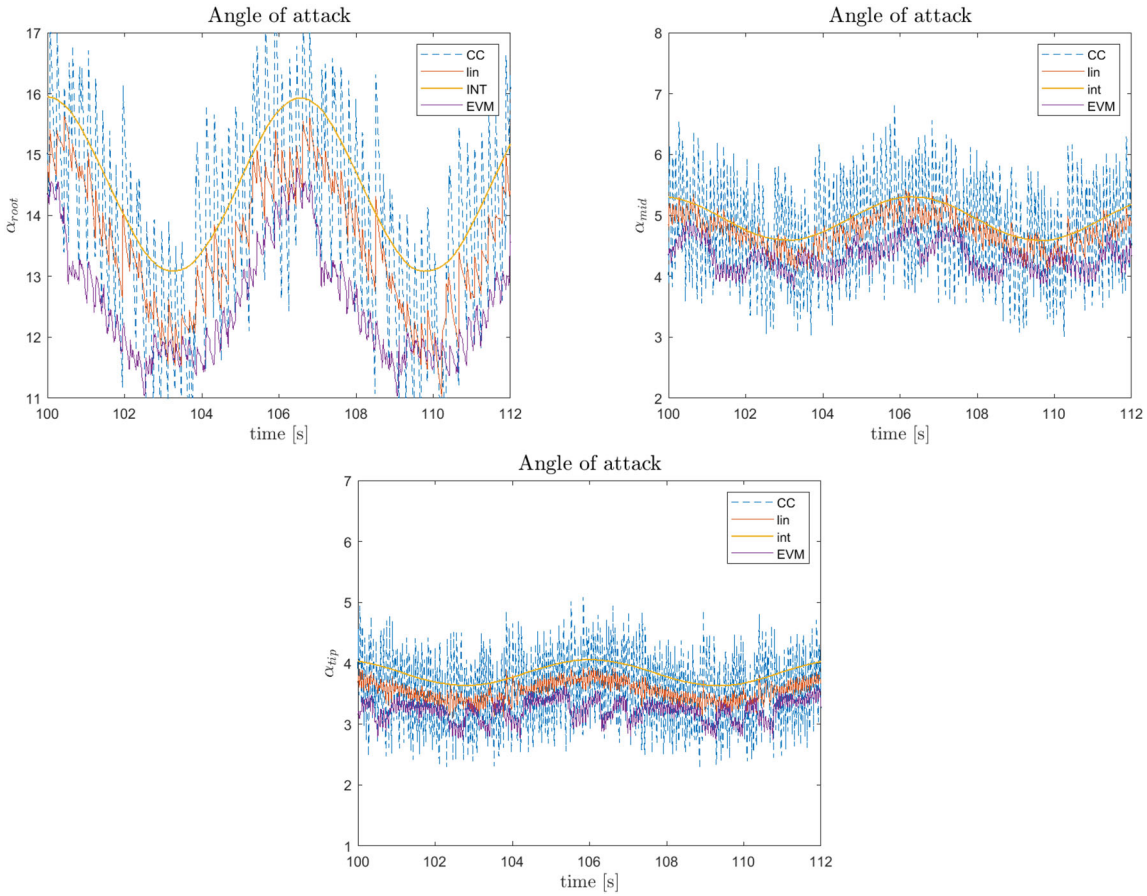

FIGURE 5 Time evolution of the angle of attack evaluated with the cell-centered (dashed blue), linear (orange), integral (yellow), and EVM (purple) approach on a point located at the root (left), mid (middle), and tip (right).

10991824, 2024, 5, Downloaded from https://onlinelibrary.wiley.com/doi/10.1002/we.2894 by Tu Delft, Wiley Online Library on [02/05/2024]. See the Terms and Conditions (https://onlinelibrary.wiley.com/terms-and-conditions) on Wiley Online Library for rules of use; OA articles are governed by the applicable Creative Commons License

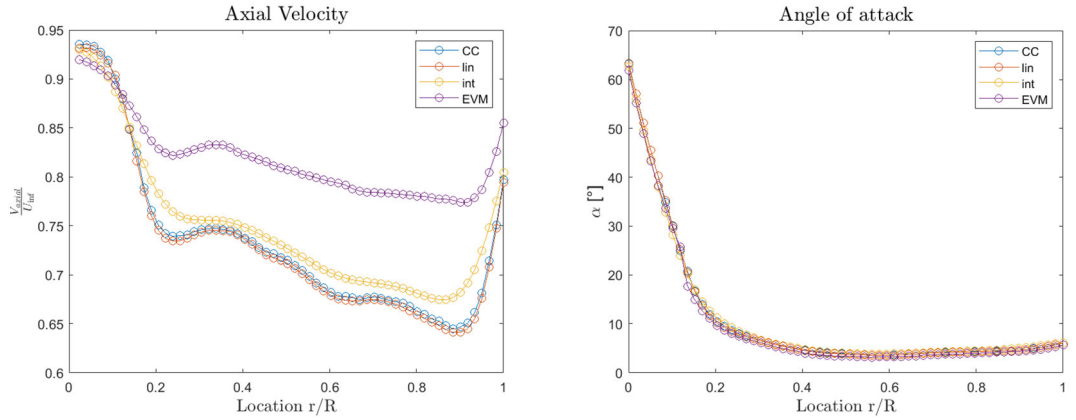

FIGURE 6 Spanwise evolution of the axial velocity (normalized with the inflow velocity) and angle of attack evaluated with the cell-centered (blue), linear (orange), integral (yellow), and EVM (purple) approach. The EVM axial velocity is the one sampled upstream and not yet projected with the new angle of attack.

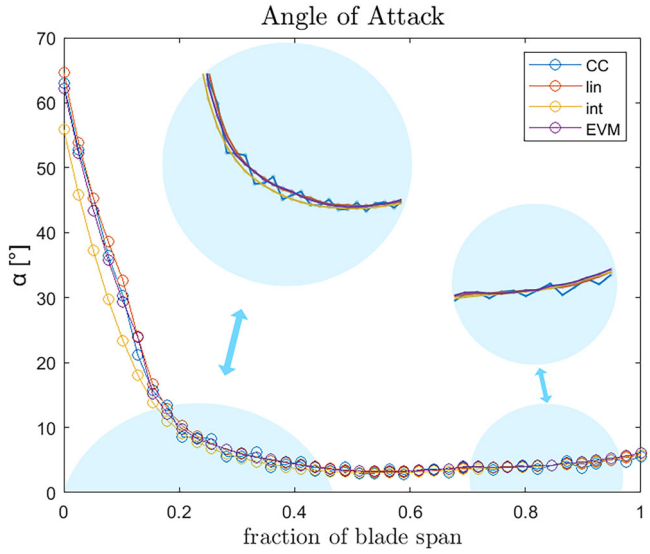

FIGURE 7 Spanwise evolution of the angle of attack, evaluated with the cell-centered, linear, integral, and EVM approach, when considering 40 points along the blade. The blue circles represent zoomed-in areas.

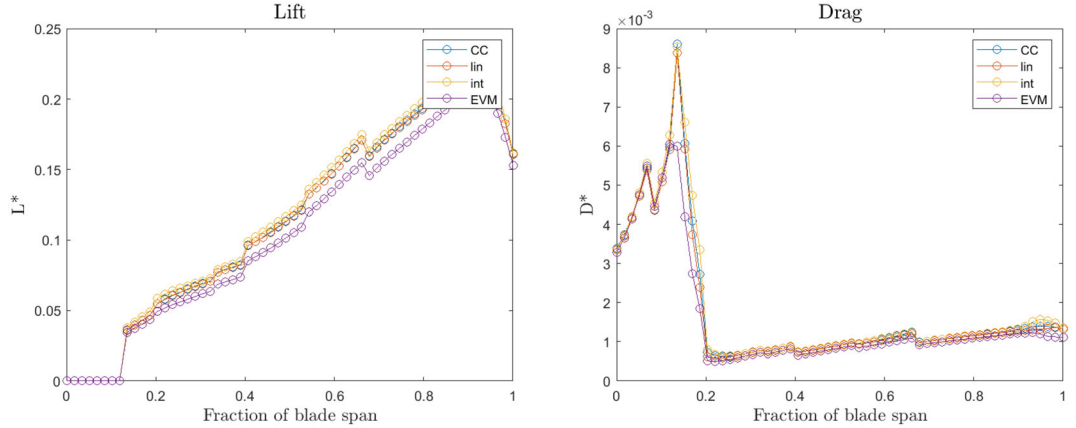

FIGURE 8 Spanwise evolution of the adimensional lift and drag forces evaluated with the cell-centered (blue), linear (orange), integral (yellow), and EVM approach (purple).

10991824, 2024, 5, Downloaded from https://onlinelibrary.wiley.com/doi/10.1002/we.2894 by Tu Delft, Wiley Online Library on [02/05/2024]. See the Terms and Conditions (https://onlinelibrary.wiley.com/terms-and-conditions) on Wiley Online Library for rules of use; OA articles are governed by the applicable Creative Commons License

Martinez-Tozzas et al[34] featured an experimental validation of the AL against experiments performed at the low-speed wind tunnel of The Norwegian University of Science and Technology.[35] Across the tested tip speed ratio (TSR) range (3, 4, 6, 9, and 12), the thrust coefficient was underpredicted by 20–25%. This is consistent with the curves represented in Figure 9, with the difference that the EVM seems to match the power perfectly. Since thrust is the quantity that most affects the wake, it is a priority to have a reliable prediction, especially when working in a wind farm environment. The EVM definitely fails at that, but so does the AL in general. One possible explanation for the thrust under prediction is that we do not model the nacelle to remain consistent with the reference study.[28] If we did, we would see a change in both aerodynamic coefficients. In particular, drag would always increase, and lift would decrease normally and increase if stall conditions occur. When drag increases, thrust does too.

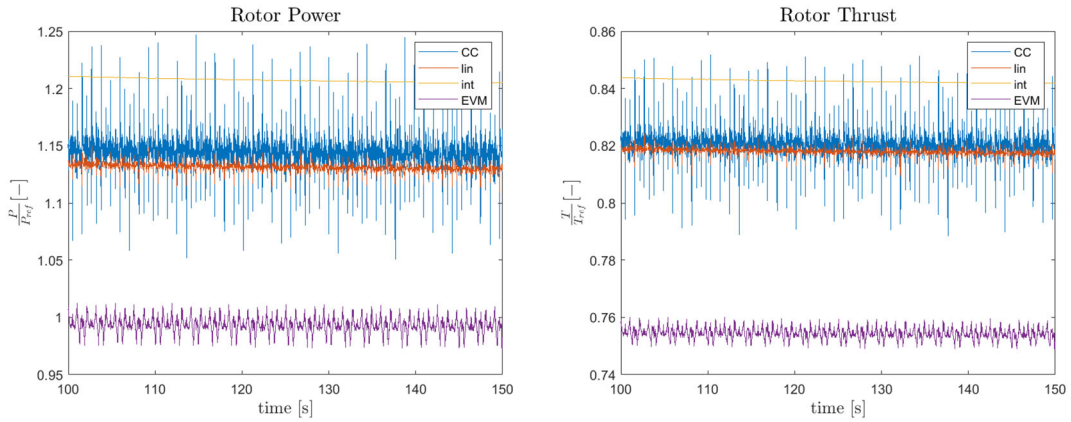

FIGURE 9 Time evolution of the rotor power and rotor axial force evaluated with the cell-centered, linear, integral, and EVM approach. Reference values from the NREL 5-MW github.[36]

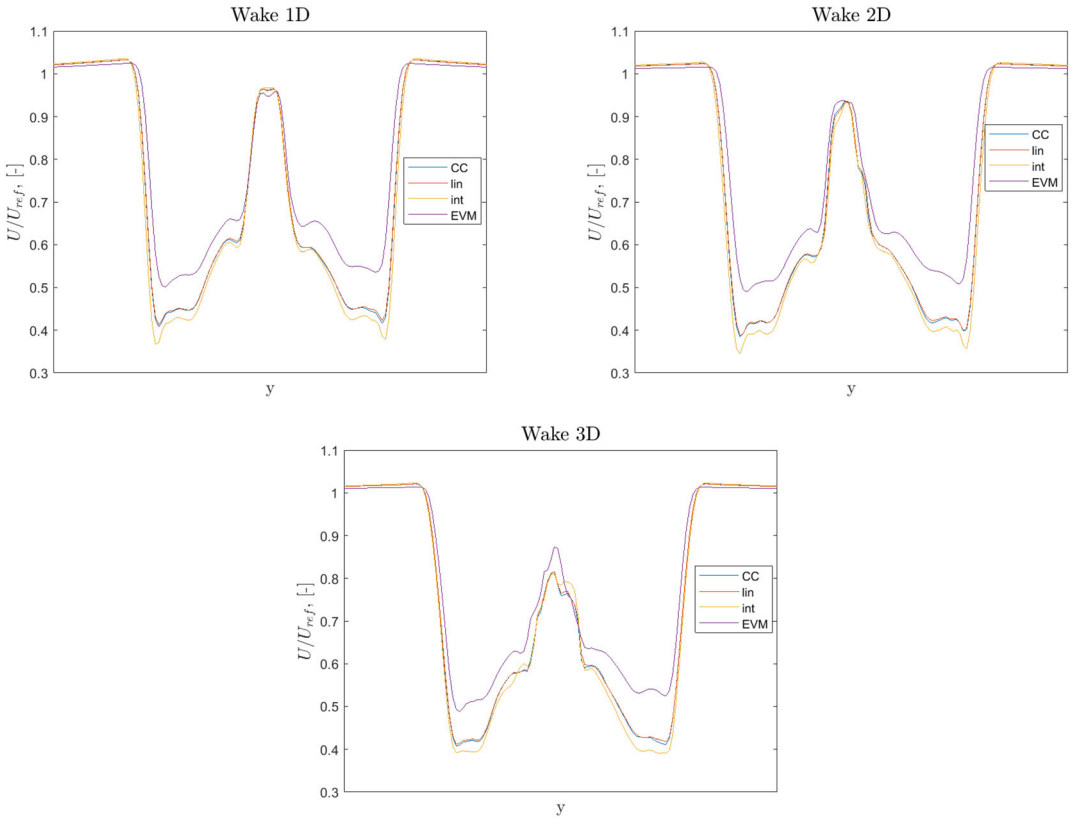

FIGURE 10 Adimensionalized wind profiles on planes parallel to the rotor plane. The planes are positioned at 1, 2, and 3 diameters downstream of the rotor, respectively.

10991824, 2024, 5, Downloaded from https://onlinelibrary.wiley.com/doi/10.1002/we.2894 by Tu Delft, Wiley Online Library on [02/05/2024]. See the Terms and Conditions (https://onlinelibrary.wiley.com/terms-and-conditions) on Wiley Online Library for rules of use; OA articles are governed by the applicable Creative Commons License

The effect of the thrust underprediction can be quantified by looking at wind profiles in the near wake. Figure 10 shows the profiles at 1, 2, and 3 diameters downstream of the rotor plane. The axial component of the velocity was averaged over the last 50 seconds of the simulation and divided by the reference wind speed of 8 m/s.

We can see that the resulting shape for the cell-centered and linear methods are almost indistinguishable.

At all distances, the lower thrust predicted by the EVM results in a smaller deficit, with the wind speed never going below half the reference one.

4.3 | Method sensitivity to force projection

We discussed in Section 1 how, together with the velocity sampling, the main issue when using hybrid CFD methods for wind turbine simulation, such as the actuator line and the actuator disk, is the choice of the regularization kernel width ϵ. The two issues are not entirely decoupled: the velocity sampled in a certain point will be influenced by a force that has been smeared with a certain regularization kernel. Previous attempts at addressing the tunability of ϵ have gone in the direction of either finding an optimal value, using it when possible[34] and correcting for it when not,[10] or projecting in a way that is more physics-informed. For example, the latter can be done by considering a kernel that is non-isotropic and has coordinates in the chord-wise, thickness-wise, and radial directions that depend on the blade chord length, the maximum thickness length, and the actuator element width and vary along the span.[4]

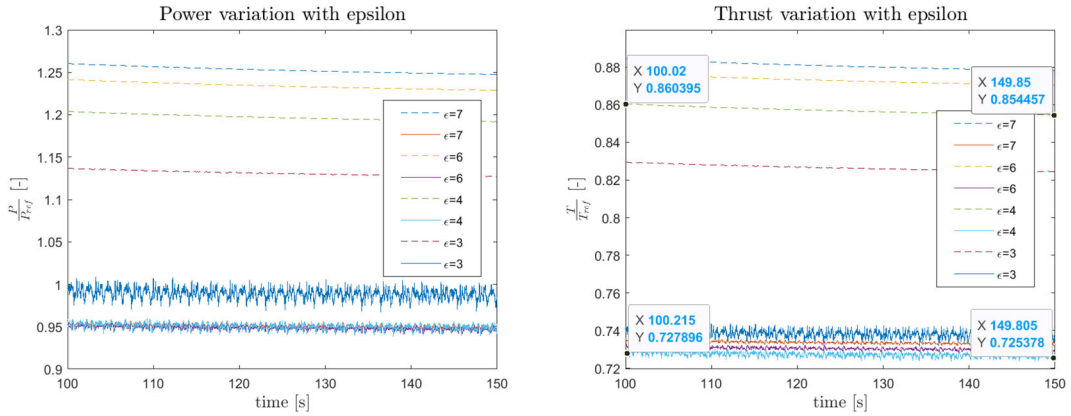

FIGURE 11 Time evolution of the rotor power and rotor axial force evaluated with the integral (dashed line) and EVM (solid line) approach with varying ϵ values. Reference values from the NREL 5-MW github.

TABLE 5 Mean power values normalized with respect to the reference in Jonkman[26] for the integral and EVM sampling with different values of ϵ.

	$\epsilon = 3$ m		$\epsilon = 4$ m		$\epsilon = 6$ m		$\epsilon = 7$ m	
	$\frac{P}{P_{ref}}$	$\Delta\%$ error	$\frac{P}{P_{ref}}$	$\Delta\%$ error	$\frac{P}{P_{ref}}$	$\Delta\%$ error	$\frac{P}{P_{ref}}$	$\Delta\%$ error
Integral	1.131	−5.51%	1.197	-	1.233	3.01%	0	4.85%
EVM	1	5.05%	0.952	-	0.949	−0.32%	0.953	0.11%

Note: The percentage errors are computed by taking, for each method, the ratio evaluated with $\epsilon = 4$ m, corresponding to a $\frac{\epsilon}{\Delta x} = 2$, as the correct one.

TABLE 6 Mean thrust values normalized with respect to the reference in Jonkman[26] for the integral and EVM sampling with different values of ϵ.

	$\epsilon = 3$ m		$\epsilon = 4$ m		$\epsilon = 6$ m		$\epsilon = 7$ m	
	$\frac{T}{T_{ref}}$	$\Delta\%$ error	$\frac{T}{T_{ref}}$	$\Delta\%$ error	$\frac{T}{T_{ref}}$	$\Delta\%$ error	$\frac{T}{T_{ref}}$	$\Delta\%$ error
Integral	0.826	−3.5%	0.856	-	0.873	1.99%	0.879	2.69%
EVM	0.740	1.78%	0.727	-	0.730	0.41%	0.734	0.96%

Note: The percentage errors are computed by taking, for each method, the ratio evaluated with $\epsilon = 4$ m, corresponding to a $\frac{\epsilon}{\Delta x} = 2$, as the correct one.

10991824, 2024, 5, Downloaded from https://onlinelibrary.wiley.com/doi/10.1002/we.2894 by Tu Delft, Wiley Online Library on [02/05/2024]. See the Terms and Conditions (https://onlinelibrary.wiley.com/terms-and-conditions) on Wiley Online Library for rules of use; OA articles are governed by the applicable Creative Commons License

Another option would be to sample in a way that makes the results more robust to the ϵ choice. In this part of the study, we decided to compare the integral and EVM sampling methods based on this characteristic.

Since the integral method finds the free-stream velocity by integrating the velocity field weighted by the force projection function, we certainly do not expect its dependence on the projection function width to be negligible. Figure 11 shows how the power and thrust vary with the choice of the ϵ/Δ_x ratio. Tables 5 and 6 add quantitative information to the qualitative one given by the figure.

Given a constant $\Delta x = 2$, the considered ϵ values are 3, 4, 6, and 7 with a value of 4 being considered as base case. Percentage errors are computed with respect to the base case results.

TABLE 7 Tested operating conditions.

	U_∞ [m/s]	ω [rpm]	$\beta[^\circ]$
Below rated 1	6	6.88	0
Below rated 2	9	10.32	0
Rated	11.4	12.1	0
Above rated 1	15	12.1	10
Above rated 2	18	12.1	15
Above rated 3	22	12.1	20

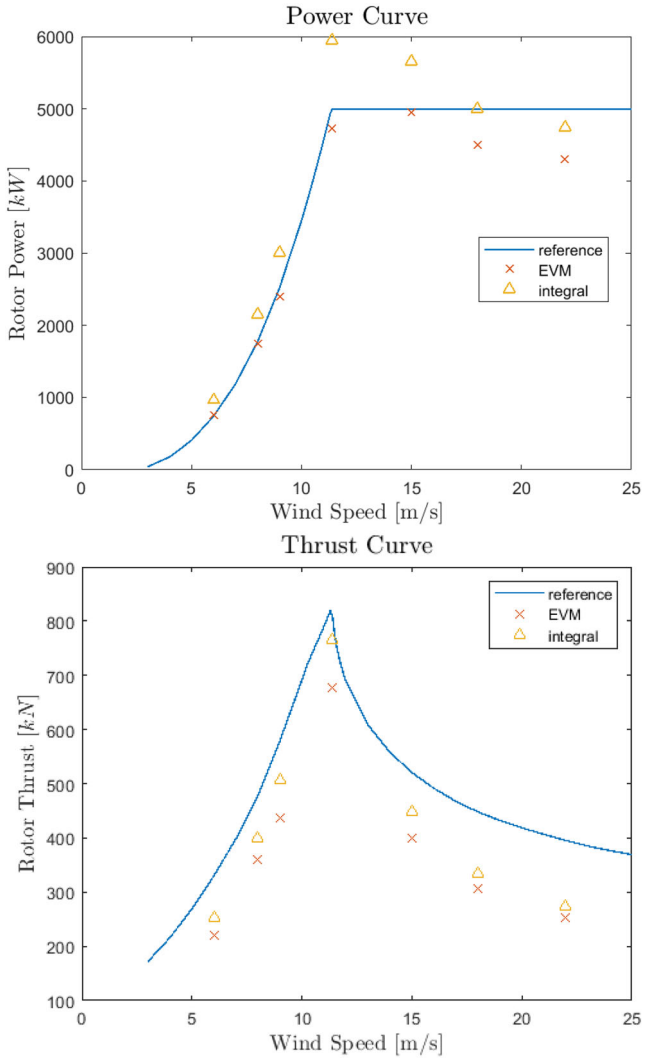

FIGURE 12 Rotor power (top) and rotor thrust (bottom) values shown for different wind speeds. The blue curves are the reference ones obtained with BEM.

10991824, 2024, 5, Downloaded from https://onlinelibrary.wiley.com/doi/10.1002/we.2894 by Tu Delft, Wiley Online Library on [02/05/2024]. See the Terms and Conditions (https://onlinelibrary.wiley.com/terms-and-conditions) on Wiley Online Library for rules of use; OA articles are governed by the applicable Creative Commons License

We can see that the EVM predicts the same power regardless of the epsilon. The only exception is the simulation with $\epsilon = 3$. This is because the $\frac{\epsilon}{\Delta x}$ ratio is lower than the minimum suggested in Mikkelsen[30] to avoid numerical issues.

Thrust predictions are less consistent (and still very inaccurate), but the advantage of using the EVM is still very clear. When plotting the power signals in time for these simulations (like in Figure 11, we also see that the EVM curves converge faster.

4.4 | Power curve

All results presented refer to the same flow and operating conditions. If we want to prove the method's robustness, a further step would be to try and match the power and thrust curves reported in Jonkman.[26] Apart from the operating condition already tested, we ran simulations across the entire operational range. It must be noted that in these simulations, we did not activate the turbine controllers and limiters present in SOWFA but rather imposed the theoretical conditions as per reference. Once the wind speed was chosen, the rotational speed was fixed based on the corresponding TSR, and the collective pitch of the blades was also modified accordingly, as detailed in Table 7.

Figure 12 shows the theoretical power and thrust curves and the predictions obtained with the EVM and the integral sampling. In the below-rated range (including the conditions considered in the rest of the study), the EVM matches the power closely and underestimates the thrust. By contrast,the integral overestimates the power (slightly) and also underestimates the thrust.

Starting from the rated condition, both methods show significantly lower accuracy in the power prediction while maintaining a similar behavior for the thrust. The overestimation of power in the above rated conditions with the integral approach is consistent with the results in Martinez-Tossaz et al.[34] The decreasing trend for the power suggests that the given pitch angle fails in avoiding stall.

5 | CONCLUSIONS

Wind farm design and control require very accurate prediction of turbine performance and wake development, and hybrid CFD-analytical models such as the actuator disk and the actuator line remain the go-to approaches to physical characterization and data retrieval for reduced-order models. However, actuator line models remain accessible only to a knowledgeable set of users because of how strongly their results depend on parameters such as the projection function width ϵ.

In this work, we have shown how a different approach to the free-stream velocity sampling can reduce this effect. The approach was validated on a well-known case and compared to the standard local sampling approach (in the cell-centered and linear variants) and the state-of-the-art integral approach (based on spatial averaging).

A study on the sensitivity of the results to the projection function width clearly shows a reduced dependency on the projection function width when using the EVM sampling. For completeness, we simulated operating conditions across the entire operational range.

The EVM consistently matches the theoretical power reference in the below-rated conditions and underestimates it for the above-rated ones. The thrust is consistently underestimated by both the EVM and the integral approach. In Section 1.4, we introduced the notion that smearing the forces generates a viscous core in the bound vorticity. The EVM implementation could benefit from accounting for the viscous core induction. This could be done by modifying the correction for the angle of attack.

We did not perform a mesh sensitivity analysis, and this limits the validity of our claims to the considered level of discretization. It is imperative for future studies to address possible mesh dependencies.

Finally, reducing the thrust mismatch should be a priority because it directly influences the wake deficit, and an accurate description of the wake is fundamental if we want to be able to use the actuator line for control purposes.

ACKNOWLEDGEMENTS

This work is part of the research programme "Robust closed-loop wake steering for large densely spaced wind farms" with project number 17512, which is (partly) financed by the Dutch Research Council (NWO). We would also like to thank Tony Martínez-Tossas from NREL for kindly providing the data necessary for the code comparison.

DATA AVAILABILITY STATEMENT

The data is available from the corresponding author upon request.

ORCID

Claudia Muscari https://orcid.org/0000-0003-4322-9721

Jan-Willem van Wingerden https://orcid.org/0000-0003-3061-7442

10991824, 2024, 5, Downloaded from https://onlinelibrary.wiley.com/doi/10.1002/we.2894 by Tu Delft, Wiley Online Library on [02/05/2024]. See the Terms and Conditions (https://onlinelibrary.wiley.com/terms-and-conditions) on Wiley Online Library for rules of use; OA articles are governed by the applicable Creative Commons License

REFERENCES

1. Bouckaert S, Pales AF, McGlade C, Remme U, Wanner B, Varro L, D'Ambrosio D, Spencer T. Net zero by 2050: A roadmap for the global energy sector; 2021.
2. Sorensen JN, Shen WZ. Numerical modeling of wind turbine wakes. *J Fluids Eng*. 2002;124(2):393-399.
3. Shen WZ, Zhu WJ, Sørensen JN. Actuator line/Navier–Stokes computations for the Mexico rotor: comparison with detailed measurements. *Wind Energy*. 2012;15(5):811-825.
4. Churchfield MJ, Schreck SJ, Martinez LA, Meneveau C, Spalart PR. An advanced actuator line method for wind energy applications and beyond. In: 35th Wind Energy Symposium IOP Publishing; 2017:1998.
5. Stevens RJAM, Martínez-Tossas LA, Meneveau C. Comparison of wind farm large eddy simulations using actuator disk and actuator line models with wind tunnel experiments. *Renew Energy*. 2018;116:470-478.
6. Troldborg N, Sorensen JN, Mikkelsen R. Numerical simulations of wake characteristics of a wind turbine in uniform inflow. *Wind Energy: An Int J Progr Appl Wind Power Convers Technol*. 2010;13(1):86-99.
7. Glauert H. *Airplane Propellers*. New York: Dover; 1985.
8. Shen WZ, Mikkelsen R, Sørensen JN, Bak C. Tip loss corrections for wind turbine computations. *Wind Energy: An Int J Progr Appl Wind Power Convers Technol*. 2005;8(4):457-475.
9. Martínez-Tossas LA, Churchfield MJ, Meneveau C. Optimal smoothing length scale for actuator line models of wind turbine blades based on Gaussian body force distribution. *Wind Energy*. 2017;20(6):1083-1096.
10. Martínez-Tossas LA, Meneveau C. Filtered lifting line theory and application to the actuator line model. *J Fluid Mech*. 2019;863:269-292.
11. Shen WZ, Sørensen JN, Zhang J. Actuator surface model for wind turbine flow computations. In: Proceedings of European Wind Energy Conference and Exhibition, Vol. 7 IOP Publishing; 2007.
12. Shives M, Crawford C. Mesh and load distribution requirements for actuator line CFD simulations. *Wind Energy*. 2013;16(8):1183-1196.
13. Dag KO. Combined pseudo-spectral/actuator line model for wind turbine applications; 2017.
14. Lamb H. *Airplane Propellers*. Cambridge: Cambridge University Press; 1932.
15. Meyer Forsting AR, Pirrung GR, Ramos-García N. A vortex-based tip/smearing correction for the actuator line. *Wind Energy Sci*. 2019;4(2):369-383.
16. Forsting ARMeyer, Troldborg N. Generalised grid requirements minimizing the actuator line angle-of-attack error. In: Journal of Physics: Conference Series, Vol. 1618 IOP Publishing; 2020:52001.
17. Kleine VG, Hanifi A, Henningson DS. Non-iterative vortex-based smearing correction for the actuator line method. *J Fluid Mech*. 2023;961:A29.
18. Xie S. An actuator-line model with Lagrangian-averaged velocity sampling and piecewise projection for wind turbine simulations. *Wind Energy*. 2021;24(10):1095-1106.
19. Schito P, Zasso A. Actuator forces in CFD: RANS and LES modeling in OpenFOAM. In: Journal of Physics: Conference Series, Vol. 524 IOP Publishing; 2014:12160.
20. Melani PF, Schito P, Persico G. Experimental assessment of an actuator-line simulation tool for VAWTS. In: Colloquium on Research and Innovation on Wind Energy on Exploitation in Urban Environment Colloquium Springer; 2018:177-200.
21. Mancini S, Boorsma K, Caboni M, Cormier M, Lutz T, Schito P, Zasso A. Characterization of the unsteady aerodynamic response of a floating offshore wind turbine to surge motion. *Wind Energy Sci*. 2020;5(4):1713-1730.
22. Gant SE. Reliability issues of les-related approaches in an industrial context. *Flow, Turbul Combust*. 2010;84:325-335.
23. Churchfield M, Lee S, Moriarty P. Overview of the simulator for wind farm application (SOWFA). National Renewable Energy Laboratory; 2012.
24. Caccialanza M, Bernini L. Development of the effective velocity model for wind turbines aerodynamics numerical simulation through an actuator line approach. 2014.
25. Bottasso C, Campagnolo F, Croce A, Maffenini L, et al. Development of a wind tunnel model for supporting research on aero-servo-elasticity and control of wind turbines. In: 13th International Conference on Wind Engineering (ICWE13); 2011:1-8.
26. Jonkman J, Butterfield S, Musial W, Scott G. Definition of a 5-mw reference wind turbine for offshore system development, National Renewable Energy Lab.(NREL), Golden, CO (United States); 2009.
27. Jonkman JM, Buhl ML, et al. *Fast User's Guide*, Vol. 365: National Renewable Energy Laboratory Golden, CO, USA; 2005.
28. Martinez-Tossas LA, Churchfield MJ, Yilmaz AE, Sarlak H, Johnson PL, Sørensen JN, Meyers J, Meneveau C. Comparison of four large-eddy simulation research codes and effects of model coefficient and inflow turbulence in actuator-line-based wind turbine modeling. *J Renew Sustain Energy*. 2018;10(3):33301.
29. Monin AS, Obukhov AM. Basic laws of turbulent mixing in the surface layer of the atmosphere. *Contrib Geophys Inst Acad Sci USSR*. 1954;151(163):e187.
30. Mikkelsen R, et al. Actuator disc methods applied to wind turbines. *Ph.D. Thesis*: Technical University of Denmark; 2003.
31. Albertson JD. *Large Eddy Simulation of Land-Atmosphere Interaction*: University of California, Davis; 1996.
32. Calaf M, Meneveau C, Meyers J. Large eddy simulation study of fully developed wind-turbine array boundary layers. *Phys Fluids*. 2010;22(1):15110.
33. Jha P, Churchfield M, Moriarty P, Schmitz S. Accuracy of state-of-the-art actuator-line modeling for wind turbine wakes. In: 51st AIAA Aerospace Sciences Meeting Including the New Horizons Forum and Aerospace Exposition; 2013:608.
34. Martínez-Tossas LA, Churchfield MJ, Leonardi S. Large eddy simulations of the flow past wind turbines: actuator line and disk modeling. *Wind Energy*. 2015;18(6):1047-1060.
35. Krogstad P-AA, Lund JA. An experimental and numerical study of the performance of a model turbine. *Wind Energy*. 2012;15(3):443-457.
36. NREL. NREL turbine models power curve archive. https://nrel.github.io/turbine-models/NREL_5MW_126_RWT.html, [Online]; 2020.

How to cite this article: Muscari C, Schito P, Viré A, Zasso A, van Wingerden J-W. The effective velocity model: An improved approach to velocity sampling in actuator line models. *Wind Energy*. 2024;27(5):447-462. doi:10.1002/we.2894

10991824, 2024, 5, Downloaded from https://onlinelibrary.wiley.com/doi/10.1002/we.2894 by Tu Delft, Wiley Online Library on [02/05/2024]. See the Terms and Conditions (https://onlinelibrary.wiley.com/terms-and-conditions) on Wiley Online Library for rules of use; OA articles are governed by the applicable Creative Commons License